



RESEARCH ARTICLE

# Exploring the effect of Ni/Cr contents on the sheet-like NiCr-oxide-decorated CNT composites as highly active and stable catalysts for urea electrooxidation

Qiuping Gan<sup>1,†</sup>, Benzhi Wang<sup>1,†</sup>, Judan Chen<sup>1</sup>, Jianniao Tian<sup>1</sup>, Tayirjan Taylor Isimjan<sup>2</sup> and Xiulin Yang<sup>1,\*</sup>

<sup>1</sup>Guangxi Key Laboratory of Low Carbon Energy Materials, School of Chemistry and Pharmaceutical Sciences, Guangxi Normal University, Guilin 541004, People's Republic of China

<sup>2</sup>Saudi Arabia Basic Industries Corporation (SABIC) at King Abdullah University of Science and Technology (KAUST), Thuwal 23955–6900, Saudi Arabia

†These authors contributed equally.

\*Corresponding author. E-mail: [xiulin.yang@kaust.edu.sa](mailto:xiulin.yang@kaust.edu.sa)

## Abstract

The developing high-efficiency urea fuel cells have an irreplaceable role in solving the increasingly severe environmental crisis and energy shortages. The sluggish six-electron dynamic anodic oxidation reaction is the bottleneck of the rapid progress of urea fuel-cell technology. To tackle this challenge, we select the NiCr bimetallic system due to the unique synergic effect between the Ni and the Cr. Moreover, better conductivity is assured using carbon nanotubes (CNTs) as the support. Most importantly, we use a simple hydrothermal method in catalyst preparation for easy scale-up at a low cost. The results show that the hybrid catalysts of NiCr<sub>x</sub>-oxide-CNTs with different Ni/Cr ratios show much better catalytic performance in terms of active surface area and current density as compared to that of Ni-hydro-CNTs. The optimized NiCr<sub>2</sub>-oxide-CNTs catalyst exhibits not only the largest electrochemically active surface area (ESA, 50.7 m<sup>2</sup> g<sup>-1</sup>) and the highest urea electrocatalytic current density (115.6 mA cm<sup>-2</sup>), but also outstanding long-term stability. The prominent performance of the NiCr<sub>2</sub>-oxide-CNTs catalyst is due to the combined effect of the improved charge transfer between Ni and Cr species, the large ESA, along with an elegant balance between the oxygen-defect sites and hydrophilicity. Moreover, we have proposed a synergistically enhanced urea catalytic mechanism.

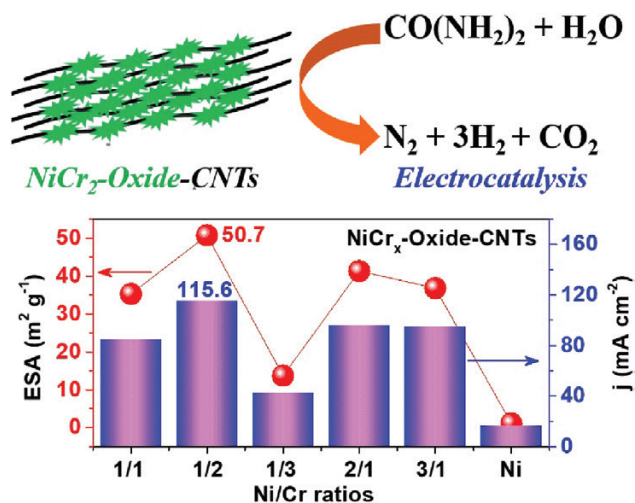
Received: 26 August 2019; Accepted: 14 November 2019

© The Author(s) 2019. Published by Oxford University Press on behalf of National Institute of Clean-and-Low-Carbon Energy

This is an Open Access article distributed under the terms of the Creative Commons Attribution Non-Commercial License

(<http://creativecommons.org/licenses/by-nc/4.0/>), which permits non-commercial re-use, distribution, and reproduction in any medium, provided the original work is properly cited. For commercial re-use, please contact [journals.permissions@oup.com](mailto:journals.permissions@oup.com)

## Graphical Abstract



**Keywords:** NiCr-oxide; coupling effect; urea electrooxidation; electrocatalysis; fuel cells

## Introduction

Growing energy demand and serious pollution issues have prompted the development of alternative environmentally friendly and sustainable energy sources [1], such as hydrogen fuel, which is an ideal replacement for conventional energy sources due to its high energy density and pollution-free products [2, 3]. Urea [ $\text{CO}(\text{NH}_2)_2$ ] has proven to be an effective  $\text{H}_2$  carrier and  $\text{CO}_2$ -storage medium for continuous energy supply due to its inherent characteristics, such as high energy density ( $16.9 \text{ MJ L}^{-1}$ ,  $10.1 \text{ wt\%}$  of  $\text{H}_2$ ), non-flammability, non-toxicity, ease of transportation and low storage cost [4, 5]. As an essential intermediate in nitrogen and carbon cycling in nature, urea is formed by combining  $\text{NH}_3$  and  $\text{CO}_2$ ; thereby, it can efficiently stabilize  $\text{NH}_3$  and fix  $\text{CO}_2$  while storing  $\text{H}_2$  with high density. The stored energy in urea can be retrieved either by releasing  $\text{H}_2$  thermally and catalytically or via a direct urea fuel cell (DUFC). The DUFC also can be used to oxidize urea-based organics from the wastewater stream to generate energy as well as pretreat the wastewater. Developing a high-performance anode catalyst is a crucial step towards achieving an efficient DUFC system.

A series of studies have shown that noble metal catalysts such as Pt- and Pd-based composites as anode materials have the high catalytic activity of the urea-oxidation reaction (UOR) [6–8]. Nevertheless, its industrial application is limited by cost and scarcity. Therefore, continued efforts are being made to find affordable, earth-abundant and non-precious-metal catalysts for UOR.

In the past few decades, researchers have discovered that Ni-based transition metal catalysts have comparable catalytic performance and stability to these of noble-metal-based catalyst for UOR. However, most Ni-based catalysts are often limited by high UOR overpotentials [9]. Moreover, two types of UOR mechanisms were reported on

Ni-based catalysts. The first one is a direct mechanism in which the intermediate nickel oxyhydroxide ( $\text{NiOOH}$ ) initiates urea oxidation in a series of electrochemical steps [10]. The other, which is an indirect mechanism proposed through density functional theory (DFT), suggests that the indirect route of urea oxidation is that the urea reacts with  $\text{NiOOH}$  to form the final product in a chemical step [11]. To address the high UOR overpotential challenge, bimetallic catalysts composed of Ni and other transition metals have been developed such as  $\text{NiCo}_2\text{O}_4$  nanowire array/Ni foam [12],  $\text{NiMoO}_4$  nanosheets [13], NiMn/carbon nanofibres [14], Ni-Mo/grapheme [15], Ni&Mn/carbon nanofibres [16], etc. The studies suggest that the bimetallic catalyst-based UOR follows both the direct- and the indirect-mechanism paths [17, 18].

Special attention needs to be paid to the NiCr bimetallic system in which Cr modifies the d-band electronic structure by weakening the Ni–O interaction, thereby improving the UOR rate [19]. Furthermore, Cr shows strong resistance towards the quaternary ammonium functional group-initiated reaction inhibition [20]. Moreover, NiCr bimetallic catalysts also show enhanced methanol oxidation and hydrogen evolution under alkaline medium [20, 21]. However, Cr-based materials have been rarely reported as catalysts for urea oxidation. A recent study revealed that 40% Cr of NiCr on carbon support exhibits a high current density of  $2933 \text{ mA mg}_{\text{Ni}}^{-1}$  for urea oxidation at a potential of 0.55 V, which is 3.6-fold higher than that of Ni/C [22]. However, the interaction between Ni and Cr is still unclear and the poor catalytic stability needs to be further improved.

Herein, we take a simple hydrothermal approach to synthesize NiCr<sub>2</sub>-oxide-carbon nanotubes (CNTs). The catalysts were characterized extensively using X-ray powder diffraction (XRD), scanning electron microscopy (SEM), transmission electron microscopy (TEM), Raman,

X-ray photoelectron spectroscopy (XPS) and electrochemical methods to achieve the best-performing catalyst in terms of electrocatalytic active surface area and electrocatalytic current density by varying the Ni/Cr ratio. The results demonstrate that NiCr<sub>2</sub>-oxide-CNTs show superior performance that gives the highest electrochemically active surface area (ESA) (50.7 m<sup>2</sup> g<sup>-1</sup>) and the highest electrocatalytic current density (115.6 mA cm<sup>-2</sup>). Moreover, the optimized catalyst reveals long-term stability for UOR in 1.0 M KOH + 0.33 M urea solution. The exceptional catalytic performance is ascribed to the fast charge-transfer kinetics, large active surface area and better dispersion of Ni nuclei [22].

## 1 Experimental

### 1.1 Materials

Chromic chloride hexahydrate (CrCl<sub>3</sub>·6H<sub>2</sub>O, ≥99%, Aladdin), nickel chloride hexahydrate (NiCl<sub>2</sub>·6H<sub>2</sub>O, ≥98%, Aladdin), ammonium fluoride (NH<sub>4</sub>F, ≥96%, Xilong), urea (CO(NH<sub>2</sub>)<sub>2</sub>, ≥99%, Aladdin), polyvinylpyrrolidone (PVP, M = 58 000, Aladdin), Nafion solution (~5%, Alfa Aesar), ethylene glycol [(CH<sub>2</sub>OH)<sub>2</sub>, XILONG], anhydrous ethanol (C<sub>2</sub>H<sub>5</sub>OH, ≥99.6%, Xilong). All reagents were of analytical grade and could be used without further purification. CNTs (>95%) were purchased from Aladdin.

### 1.2 Synthesis of NiCr<sub>x</sub>-oxide-CNTs composites

The NiCr<sub>2</sub>-oxide-CNTs hybrid composites were obtained through the hydrothermal method as follows: 73.3 mg NiCl<sub>2</sub>·6H<sub>2</sub>O, 163.5 mg CrCl<sub>3</sub>·6H<sub>2</sub>O, 0.277 8 g NH<sub>4</sub>F, 0.225 2 g CO(NH<sub>2</sub>)<sub>2</sub>, 100 mg PVP and 100 mg CNTs were added to a continuous sonication solution of 20 mL H<sub>2</sub>O/ethylene glycol (v/v = 1/1). After 30 min, the resulting suspension was transferred to Teflon-lined stainless steel and autoclaved for 9 h at 120°C. The resulting products were centrifuged at 6000 rpm for 10 min, rinsed with excess H<sub>2</sub>O/ethanol and freeze-dried over 12 h. The obtained products were nominated as NiCr<sub>2</sub>-oxide-CNTs. As a comparison, a series of NiCr<sub>x</sub>-oxide-CNTs composites with different Ni/Cr molar ratios (1/1, 1/3, 2/1 and 3/1) were further prepared using a similar approach, as mentioned above. Meanwhile, the best-performing catalyst was also made using direct hydrothermal methods for comparison purposes.

### 1.3 Characterizations

The morphology and microstructure of the catalyst were investigated in detail by SEM (FEI Quanta 200 FEG) and TEM (JEM-2100F) with X-ray energy dispersive spectroscopy (EDS). The crystal structure of the material was characterized by XRD (Rigaku D/Max 2 500 V/PC) at a scan speed of 2.0 degree min<sup>-1</sup>. Thermal gravimetric measurement was made on a TGA/STA409 PC module with a rising

temperature rate of 2.5°C min<sup>-1</sup> from 20 to 800°C under continuous O<sub>2</sub> flow. The true ratio of the different metals in the catalyst was examined by inductively coupled plasma atomic emission spectrometry (ICP-AES, IRIS Intrepid II XSP). The chemical states of the different elements were probed by XPS (JPS-9 010 Mg Kα). The binding energy was calibrated based on a 284.8-eV (C–C bond) of the C 1s peak and a standard deviation of approximately ±0.05 eV. The true ratios of Ni and Cr for different materials were determined by inductively coupled plasma (ICP, PekinElmer FLexar-NexION300X).

### 1.4 Electrochemical measurements

All electrochemical measurements were performed in a standard three-electrode cell with a multi-channel Biologic VMP3 as an electrochemical workstation, in which a glassy carbon electrode (GCE), graphite plate and saturated calomel electrode (SCE) were used as the working, counter and reference electrodes, respectively. Before the experiment, several GCEs were polished with Al<sub>2</sub>O<sub>3</sub> fine powder, then washed with H<sub>2</sub>SO<sub>4</sub>, ethanol and H<sub>2</sub>O three times. The working electrode was prepared as follows: 4.0 mg of the catalytic material was ultrasonically dispersed in 1.0 mL mixed solvent (32 μL of 5% Nafion + 200 μL of ethanol + 768 μL of H<sub>2</sub>O) for 30 min to form a homogeneous solution. Then, 10 μL of the above catalyst inks was pipetted onto the surface of the GCE (φ = 3 mm) and naturally dried for use. The loading of the catalyst was about 0.566 mg cm<sup>-2</sup>. Cyclic voltammetry (CV) was analysed in the potential range of 0.0 to 0.8 V (vs. SCE) with a scan rate of 50 mV s<sup>-1</sup> in 1.0 M KOH saturated with N<sub>2</sub> with and without 0.33 M urea electrolyte. Since the concentration of urea in human urine is approximately 0.33 M and most previous reports on the electrocatalysis of urea were carried out in 1.0 M KOH solution, the urea concentration of 0.33 M was used for comparison purposes in this work [23–25]. The stability of the catalyst was tested by chronoamperometry at a fixed potential of 0.45 V (vs. SCE) for 2.0 h in a 1.0 M KOH + 0.33 M urea solution. All electrochemical studies were conducted at room temperature (25 ± 1°C).

## 2 Results and discussion

### 2.1 Crystal structure and thermogravimetric analysis

The sheet-like NiCr<sub>2</sub>-oxide-CNTs was synthesized by a facile one-step method, in which the precursors of NiCl<sub>2</sub>, CrCl<sub>3</sub>, CNTs, NH<sub>4</sub>F, PVP and urea were ultrasonically dispersed in a mixed solution of H<sub>2</sub>O-ethylene glycol and then heated to 120°C for 9 h to achieve the final composite (Fig. 1a). Studies have shown that urea provides an alkaline environment, PVP and ethylene glycol manipulate microstructures as ligands, while NH<sub>4</sub>F regulates the directional growth.

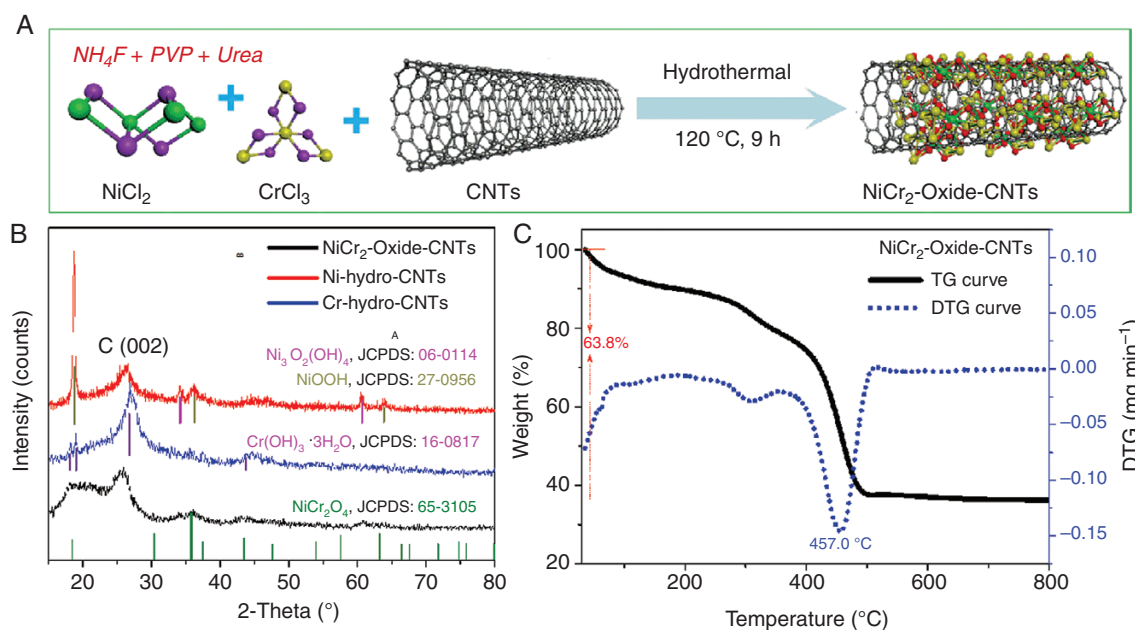


Fig. 1: (a) Schematic illustration of the preparation of  $\text{NiCr}_2$ -oxide-CNTs composite. (b) XRD patterns of  $\text{NiCr}_2$ -oxide-CNTs, Ni-hydro-CNTs and Cr-hydro-CNTs. (c) Thermogravimetric (TG) and differential thermogravimetric (DTG) curves of  $\text{NiCr}_2$ -oxide-CNTs with a heating rate of  $2.5^\circ\text{C min}^{-1}$  under  $\text{O}_2$  atmosphere.

The XRD patterns of the optimized catalyst  $\text{NiCr}_2$ -oxide-CNTs with the two catalysts prepared using hydrothermal methods in the absence of either Ni (Cr-hydro-CNTs) or Cr (Ni-hydro-CNTs) are shown in Fig. 1b. The rest of the  $\text{NiCr}_x$ -oxide-CNTs catalysts show similar XRD patterns [Fig. S1 in the online Supplementary Data (see the online Supplementary Data)]. Fig. 1b indicates that the crystal structures of  $\text{NiCr}_2$ -oxide-CNTs are consistent with the standard model of  $\text{NiCr}_2\text{O}_4$  (JCPDS: 65–3 105) [26], including the typical peak of the crystal plane (002) of CNTs at  $25.8^\circ$ . Notably, the Cr-hydro-CNTs exhibits four characteristic diffraction peaks at  $18.2$ ,  $19.4$ ,  $26.6$  and  $43.7^\circ$  corresponding to the (001), (100), (101) and (201) crystal planes of  $\text{Cr}(\text{OH})_3 \cdot 3\text{H}_2\text{O}$  (JCPDS: 16–0 817) [27]. Simultaneously, the XRD pattern of Ni-hydro-CNTs matches well with the standard models of  $\text{NiOOH}$  (JCPDS: 27–0 956) and  $\text{Ni}_3\text{O}_2(\text{OH})_4$  (JCPDS: 06–0 114) as well, suggesting the co-existence of these two species in Ni-hydro-CNTs composite. The ICP test results of  $\text{NiCr}_x$ -oxide-CNTs samples with different molar ratios of Ni/Cr indicate a high level of consistency between the experimental values and the theoretical values [Table S1 in the online Supplementary Data (see the online Supplementary Data)].

Thermogravimetric (TG) and differential thermogravimetric (DTG) curves were applied to explore the oxide content of the optimal  $\text{NiCr}_2$ -oxide-CNTs catalyst under  $\text{O}_2$  atmosphere (Fig. 1c). In the initial stage from room temperature to around  $120^\circ\text{C}$ , the weight loss is due to the evaporation of water. Then, a significant drop between  $400$  and  $600^\circ\text{C}$  is attributed to the oxidation of carbon. In addition, the 36.2 wt% remnant of  $\text{NiCr}_2$ -oxide-CNTs after  $800^\circ\text{C}$  is nickel-chromium oxide [28]. Notably, there is a sharp exothermic peak on the DTG curve at

$457.0^\circ\text{C}$  caused by oxidative pyrolysis of CNTs [29]. As shown in Fig. S2 in the online Supplementary Data (see the online Supplementary Data), the sharp Raman peaks of  $\text{NiCr}_2$ -oxide-CNTs, Ni-hydro-CNTs and Cr-hydro-CNTs are observed at  $\sim 1341$  and  $1582\text{ cm}^{-1}$  for the D and G bands where the ratio of the D and G bands refers to the graphitic degree [30]. One can conclude that the  $\text{NiCr}_2$ -oxide-CNTs have the highest defect structure due to the highest  $I_D/I_G$  value (1.18) as compared to these of Ni-hydro-CNTs (1.13) and Cr-hydro-CNTs (1.06).

## 2.2 Morphology analysis

The morphology and microstructure of  $\text{NiCr}_2$ -oxide-CNTs were further investigated by SEM image, TEM images and EDS mappings. Fig. 2a is an SEM image which shows that some spherical structural species are intertwined with CNTs. The TEM image of Fig. 2b further discloses the spherical species composed of sheet-like species containing two types of clear lattice stripes with the lattice spacings of about  $0.25$  and  $0.32\text{ nm}$  (Fig. 2c), which are consistent with the (311) facet of  $\text{NiCr}_2\text{O}_4$  and (002) facet of CNTs, respectively [31]. Moreover, the EDS mappings manifest that the elements of Ni, Cr and O are evenly distributed throughout the entire skeleton of the  $\text{NiCr}_2$ -oxide-CNTs composite (Fig. 2d).

## 2.3 XPS analysis

XPS analysis was adopted to probe the chemical states of Ni and Cr elements in  $\text{NiCr}_2$ -oxide-CNTs (Fig. 3). As shown in Fig. S3a in the online Supplementary Data (see the online Supplementary Data), the survey XPS spectra showed

that NiCr<sub>x</sub>-oxide-CNTs with different Ni/Cr ratios contained Ni, Cr, C and O elements. The high-resolution C 1s [Fig. S3b in the online Supplementary Data (see the online Supplementary Data)] of each catalyst consists of four peaks at C=C (284.0 eV), C-C (284.8 eV), C-O (286.0 eV) and C=O (288.8 eV) [32], which are used as calibration standards. As shown in Fig. 3a, the high-resolution Ni 2p spectrum of NiCr<sub>2</sub>-oxide-CNTs has been deconvoluted into four peaks, in which the binding energies at 854.9 and 872.7 eV are ascribed to Ni 2p<sub>3/2</sub> and Ni 2p<sub>1/2</sub>, respectively, and the other two peaks are attributed to satellite peaks [33, 34]. All of these characteristics indicate that the Ni species in the composite is mainly present as Ni<sup>2+</sup>. It is worth noting that the binding energy of Ni 2p<sub>3/2</sub> in the NiCr<sub>2</sub>-oxide-CNTs composite has a negative shift of 0.25 eV compared to that of Ni-hydro-CNTs. Meanwhile, the high-resolution Cr 2p region of the NiCr<sub>2</sub>-oxide-CNTs composite was fitted to

two peaks corresponding to Cr 2p<sub>3/2</sub> (576.4 eV) and Cr 2p<sub>1/2</sub> (586.2 eV) of Cr<sup>3+</sup> [33], respectively (Fig. 3b). The binding energy of Cr 2p<sub>3/2</sub> for NiCr<sub>2</sub>-oxide-CNTs exhibits a positive shift of 0.18 eV as compared to that of Cr-hydro-CNTs. The binding-energy changes indicate the presence of electronic-coupling and electron-transfer effects between the components of NiCr<sub>2</sub>-oxide-CNTs [35, 36]. The electron migration between Ni and Cr is believed to promote the electrooxidation of urea synergistically [37]. The high-resolution Ni 2p and Cr 2p of the rest of the NiCr<sub>x</sub>-oxide-CNTs composites were also analysed for comparison [Fig. S3c and d in the online Supplementary Data (see the online Supplementary Data)], which show a similar electronic structure. In addition, the high-resolution O 1s of all composites are fitted to four peaks representing metal-oxide, vacancies, C-O and adsorbed H<sub>2</sub>O (Fig. 3c), respectively [38]. The results reveal that the Cr species has a positive effect on the oxygen-defect sites, while the Ni species increase the hydrophilicity of the composite. As a result, the excellent urea electrocatalytic activity of the optimized NiCr<sub>2</sub>-oxide-CNTs is the fruit of an elegant balance between the oxygen-defect sites and hydrophilicity.

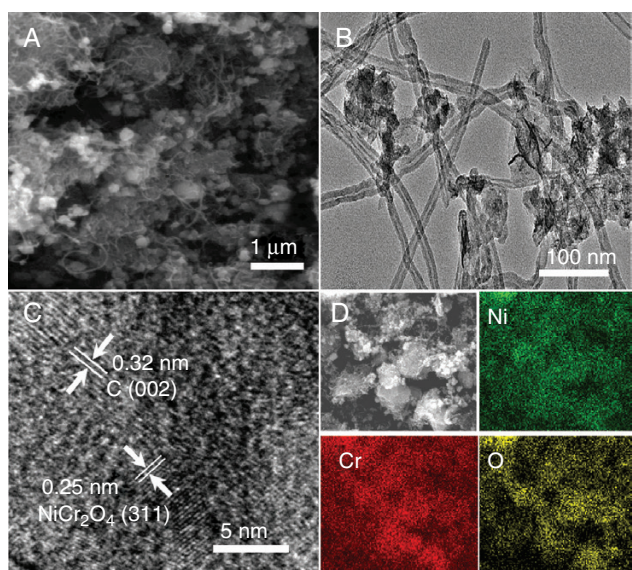


Fig. 2: (a) SEM, (b) TEM and (c) high-resolution TEM images of NiCr<sub>2</sub>-oxide-CNTs. (d) EDS mappings of NiCr<sub>2</sub>-oxide-CNTs with Ni, Cr and O elements

#### 2.4 Electrochemical performance analysis

The CV curves of NiCr<sub>x</sub>-oxide-CNTs, Ni-hydro-CNTs and Cr-hydro-CNTs performed in 1.0 M KOH solution were used to evaluate their ESA (Fig. 4a). The figures indicate that all catalysts except Cr-hydro-CNTs present a pair of redox peaks in the potential range of 0.0 to 0.8 V. The anode peak in the forward scan is consistent with the Ni(OH)<sub>2</sub> species oxidized to NiOOH and the cathode peak in the reverse scan is ascribed to the reduction of NiOOH to Ni(OH)<sub>2</sub> [11, 39]. Generally, the ESA was calculated by the required reduction charge in the reverse scan, which is directly proportional to the number of active sites for urea electrooxidation. The ESA values of all catalysts can be estimated from the equation  $ESA = Q/mq$  [38, 40], where Q is the total charge used for the reduction

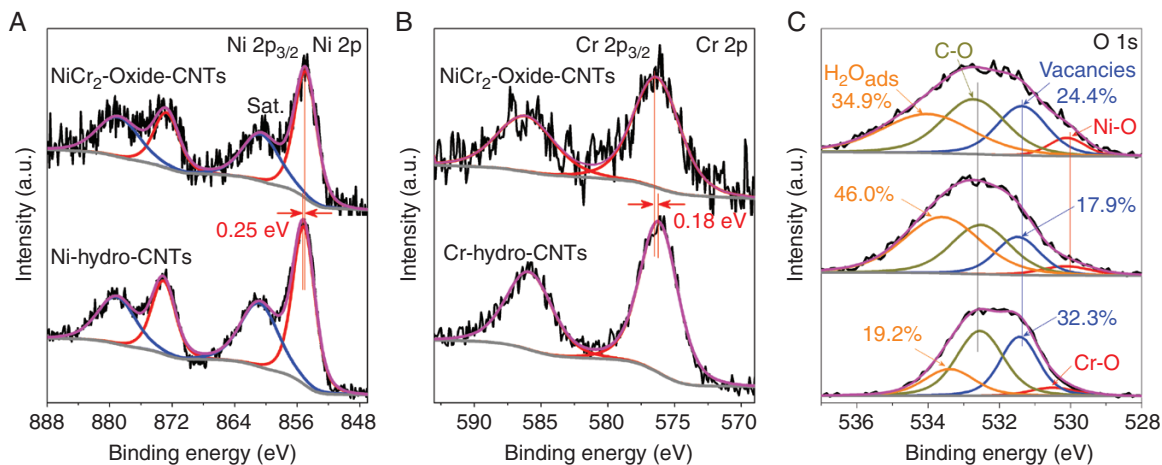


Fig. 3: High-resolution XPS regions of (a) Ni 2p, (b) Cr 2p and (c) O 1s from NiCr<sub>2</sub>-oxide-CNTs, Ni-hydro-CNTs and Cr-hydro-CNTs

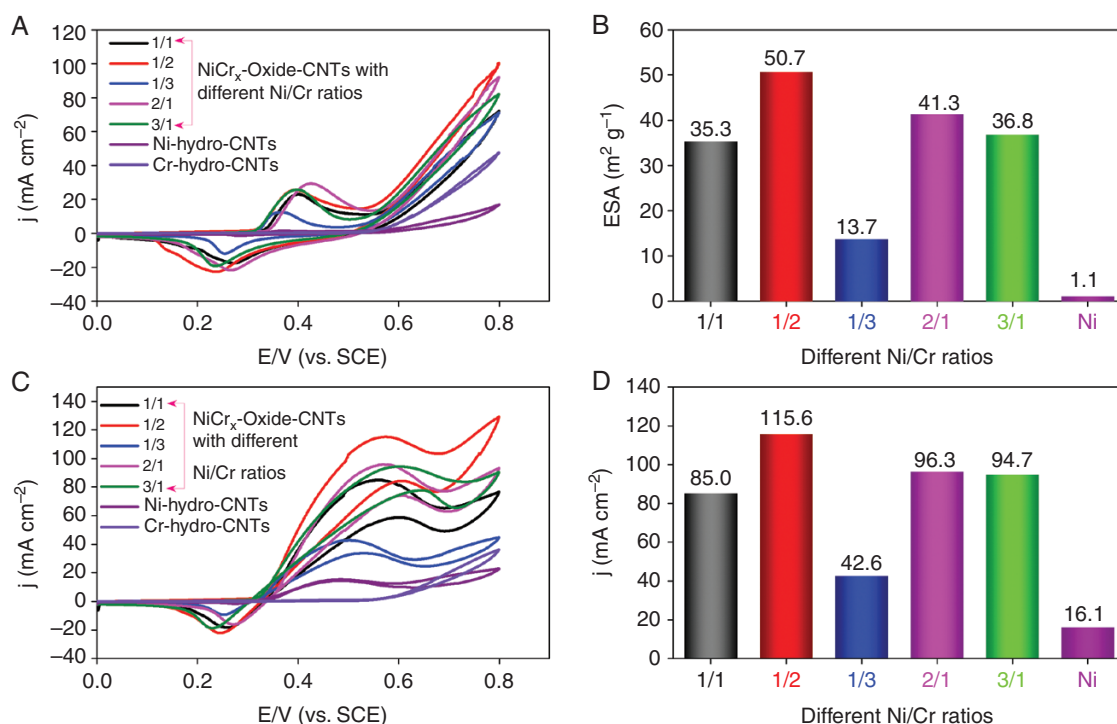


Fig. 4: (a) CV curves of NiCr<sub>x</sub>-oxide-CNTs with different Ni/Cr ratios, Ni-hydro-CNTs and Cr-hydro-CNTs in 1.0 M KOH. (b) The summarized ESA values from (a). (c) CV curves of different catalysts in 1.0 M KOH + 0.33 M urea. (d) The summarized forward current densities from (c).

of NiOOH species to Ni(OH)<sub>2</sub>,  $m$  is the mass of Ni in the supported catalyst and  $q$  is 257  $\mu\text{C cm}^{-2}$  as only one electron for NiOOH converted to Ni(OH)<sub>2</sub>. As shown in Fig. 4b, the NiCr<sub>2</sub>-oxide-CNTs shows the highest ESA of 50.7  $\text{m}^2 \text{g}^{-1}$ , which is 1.44-, 3.70-, 1.23-, 1.37- and 46-fold higher than NiCr-oxide-CNTs (35.3  $\text{m}^2 \text{g}^{-1}$ ), NiCr<sub>3</sub>-oxide-CNTs (13.7  $\text{m}^2 \text{g}^{-1}$ ), Ni<sub>2</sub>Cr-oxide-CNTs (41.3  $\text{m}^2 \text{g}^{-1}$ ), Ni<sub>3</sub>Cr-oxide-CNTs (36.8  $\text{m}^2 \text{g}^{-1}$ ) and Ni-hydro-CNTs (1.1  $\text{m}^2 \text{g}^{-1}$ ). Studies have found that the introduction of a certain amount of Cr species can expose more active sites through synergistic interactions of Ni and Cr species [41]. Moreover, the various Ni/Cr ratios result in different morphology in NiCr<sub>x</sub>-oxide-CNTs composites, which also have a significant effect on ESA values [21]. Therefore, the optimal value of the Ni/Cr ratio is required to obtain the highest ESA. Thereafter, the electrocatalytic tests of all catalysts were performed in 1.0 M KOH + 0.33 M urea (Fig. 4c). Although all catalysts show a similar onset potential at  $\sim 0.32 \text{ V}$  except for Cr-hydro-CNTs (0.56 V), the NiCr<sub>2</sub>-oxide-CNTs catalyst has the largest current density (115.6  $\text{mA cm}^{-2}$ ), which is about 1.36-, 2.71-, 1.20-, 1.22- and 7.2-fold higher than those of NiCr-oxide-CNTs, NiCr<sub>3</sub>-oxide-CNTs, Ni<sub>2</sub>Cr-oxide-CNTs, Ni<sub>3</sub>Cr-oxide-CNTs and Ni-hydro-CNTs, respectively (Fig. 4d). Here, the higher onset potential of the Cr-hydro-CNTs catalyst than others may be due to the fact that the catalyst lacks effective active sites to adsorb urea molecules, thereby requiring a higher polarization potential to drive the reaction. It is also worth noting that Cr-hydro-CNTs has almost no catalytic activity for urea, but the composite catalysts including Ni and Cr possess

higher catalytic performance as compared to both Ni and Cr single-component catalysts for urea oxidation, once again indicating the synergistic effect between Ni and Cr species. In addition, we also studied the electrochemical performance of NiCr<sub>2</sub>-oxide, CoCr<sub>2</sub>-oxide-CNTs and FeCr<sub>2</sub>-oxide-CNTs in 1.0 M KOH and 1.0 M KOH + 0.33 M urea [Fig. S4 in the online Supplementary Data (see the online Supplementary Data)]. The results show that the catalytic performances of these control catalysts are much lower than that of NiCr<sub>2</sub>-oxide-CNTs, which indicates not only the importance of the CNTs, but also the unique effect of synergy between Ni and Cr towards the catalytic performance of urea oxidation.

In the initial stage of electrocatalysis, studies found that the Ni(OH)<sub>2</sub> species first lose one electron to form NiOOH on the catalyst surface [Ni(OH)<sub>2</sub>+OH<sup>-</sup> ↔ NiOOH+H<sub>2</sub>O+e<sup>-</sup>] [42, 43]. Subsequently, the produced NiOOH intermediates could adsorb hydroxyl ions and urea molecules from the electrolyte. After undergoing a complex multi-electron-transfer process, the urea molecules are finally oxidized to N<sub>2</sub>, CO<sub>2</sub> and H<sub>2</sub>O on the active sites [CO(NH<sub>2</sub>)<sub>2</sub>+6OH<sup>-</sup> → CO<sub>2</sub>+N<sub>2</sub>+5H<sub>2</sub>O+6e<sup>-</sup>] [38, 44] while the NiOOH species is reduced back to Ni(OH)<sub>2</sub> species [45]. The summarized forward current densities of NiCr<sub>x</sub>-oxide-CNTs are shown in Fig. 4d; the NiCr<sub>2</sub>-oxide-CNTs shows the highest current density. Furthermore, it is also among the top-performing urea-oxidation catalysts reported in the literature because of the low onset potentials and high peak current densities [Table S2 in the online Supplementary Data (see the online Supplementary Data)].

The stabilities of NiCr<sub>x</sub>-oxide-CNTs catalysts with different Ni/Cr ratios were tested by chronoamperometry at a constant potential of 0.45 V in 1.0 M KOH + 0.33 M urea electrolyte. As shown in Fig. 5, the NiCr<sub>2</sub>-oxide-CNTs catalyst shows the highest initial current density (85.0 mA cm<sup>-2</sup>) and limiting current density (38.6 mA cm<sup>-2</sup>). The initial spike can be attributed to the higher urea concentration on the surface of the catalysts at the beginning and the current stabilizes after some time where the system reaches the equilibrium [46].

## 2.5 Catalytic-mechanism analysis

As discussed above, the NiCr<sub>2</sub>-oxide-CNTs catalyst exhibits excellent electrocatalytic performance for urea oxidation. Electrochemical studies show that the Ni<sup>2+</sup> species on the surface of the NiCr<sub>2</sub>-oxide-CNTs catalyst is first oxidized to NiOOH species (lose 1e<sup>-</sup>) as the active sites (M) (Fig. 6, Step I). Then, the urea molecules in the solution are adsorbed into the active sites of the NiOOH surface and the partially positively charged H atoms of the urea molecules are adsorbed onto the surface of the negatively charged Cr species (due to a higher electron density than Ni species) through electrostatic interaction (Step II). After the attack of OH<sup>-</sup> ions and the combination of electrooxidation (loss of 1e<sup>-</sup>), one H atom is removed to form a free H<sub>2</sub>O molecule (Step III). After three consecutive dehydrations, an intermediate state of M-CO-N<sub>2</sub> is formed. Similarly, after an OH<sup>-</sup> attack and the electrooxidation (loss of 1e<sup>-</sup>) followed by losing of a N<sub>2</sub>, another intermediate state of M-CO-OH is formed (Step IV). Along with the further attack of OH<sup>-</sup> ions and one more electrooxidation process (loss of 1e<sup>-</sup>), the last intermediate state of M-CO<sub>2</sub> is formed while releasing one molecule of H<sub>2</sub>O (Step V). Finally, the active site M is recovered by releasing CO<sub>2</sub> (Step VI) [11, 43].

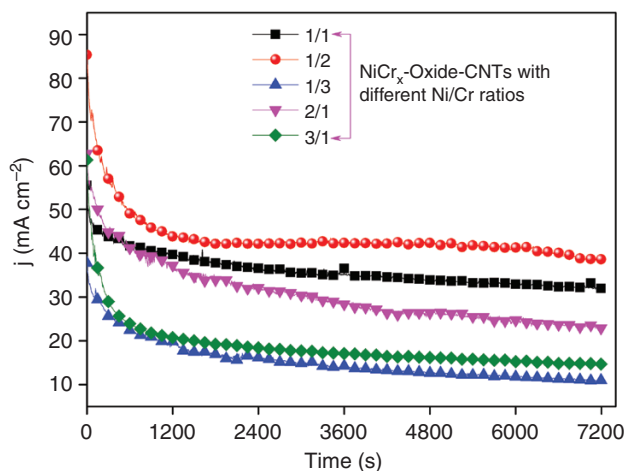


Fig. 5: Chronoamperometric curves of NiCr<sub>x</sub>-oxide-CNTs catalysts with different Ni/Cr ratios at a constant potential of 0.45 V (vs. SCE) in 1.0 M KOH + 0.33 M urea for keeping 7200 s

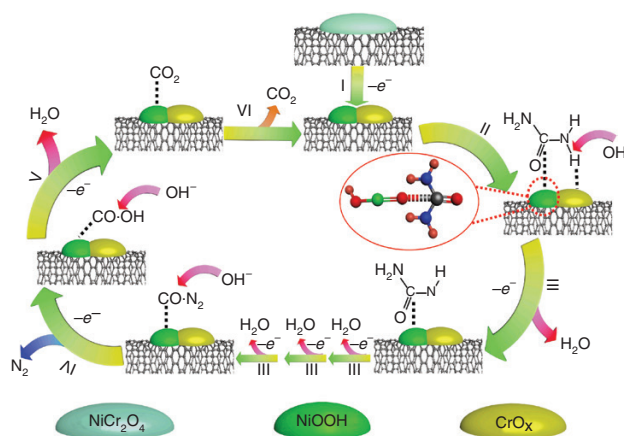


Fig. 6: The proposed possible catalytic mechanism of the electrocatalytic urea oxidation by NiCr<sub>x</sub>-oxide-CNTs catalyst in alkaline media

## 3 Conclusion

In summary, the NiCr<sub>x</sub>-oxide-CNTs with different Ni/Cr ratio catalysts were prepared by a facile hydrothermal method. Various techniques were applied to investigate the crystal structures, morphologies and chemical states. The results indicate that the NiCr<sub>2</sub>-oxide-CNTs composite is composed of the sheet-like structure of NiCr<sub>2</sub>-oxide and CNTs. There is a visible synergistic effect between Ni and Cr. The electrochemical studies show that the NiCr<sub>2</sub>-oxide-CNTs catalyst exhibits the immense ESA value (50.7 m<sup>2</sup> g<sup>-1</sup>), highest current density (115.6 mA cm<sup>-2</sup>) and permanent stability for urea electrooxidation in alkaline medium. The prominent performance of the NiCr<sub>2</sub>-oxide-CNTs catalyst is mainly ascribed to its improved charge-transfer kinetics, the larger ESA, along with an elegant balance between the oxygen-defect sites and hydrophilicity. Moreover, the results also demonstrate a promising application of the non-noble-metal catalysts in water splitting, hydrogen production, fuel cells, etc.

## Supplementary data

Supplementary data is available at Clean Energy online.

## Acknowledgements

This work has been supported by the National Natural Science Foundation of China (21965005), Natural Science Foundation of Guangxi Province (2018GXNSFAA294077, 2017GXNSFGA198004), Project of High-Level Talents of Guangxi (F-KA18015, 2018ZD004) and Innovation Project of Guangxi Graduate Education (XYCSZ2019056, YCBZ2019031).

## Conflict of Interest

None declared.

## Reference

- [1] Xiao C, Li S, Zhang X, et al. MnO<sub>2</sub>/MnCo<sub>2</sub>O<sub>4</sub>/Ni heterostructure with quadruple hierarchy: a bifunctional electrode architecture for overall urea oxidation. *J Mater Chem A* 2017; 5:7825–32.
- [2] Jian Y, Bingxu C, Xiaokang L, et al. Efficient and robust hydrogen evolution: phosphorus nitride imide nanotubes as supports for anchoring single ruthenium sites. *Angew Chem Int Ed* 2018; 57:1–7.
- [3] Hou M, Teng X, Wang J, et al. Multiscale porous molybdenum phosphide of honeycomb structure for highly efficient hydrogen evolution. *Nanoscale* 2018; 10:14594–9.
- [4] Wang D, Vijapur SH, Wang Y, et al. NiCo<sub>2</sub>O<sub>4</sub> nanosheets grown on current collectors as binder-free electrodes for hydrogen production via urea electrolysis. *Int J Hydrogen Energy* 2017; 42:3987–93.
- [5] Wang X, Wang J, Sun X, et al. Hierarchical coral-like NiMoS nano-hybrids as highly efficient bifunctional electrocatalysts for overall urea electrolysis. *Nano Res* 2017; 11:988–96.
- [6] Mohamed IMA, Yasin AS, Barakat NAM, et al. Electrocatalytic behavior of a nanocomposite of Ni/Pd supported by carbonized PVA nanofibers towards formic acid, ethanol and urea oxidation: a physicochemical and electro-analysis study. *Appl Surf Sci* 2018; 435:122–9.
- [7] Urbańczyk E, Jaroń A, Simka W. Electrocatalytic oxidation of urea on a sintered Ni–Pt electrode. *J Appl Electrochem* 2017; 47:133–8.
- [8] Yoon J, Lee D, Lee YN, et al. Solid solution palladium-nickel bimetallic anode catalysts by co-sputtering for direct urea fuel cells (DUFC). *J Power Sources* 2019; 431:259–64.
- [9] King RL, Botte GG. Hydrogen production via urea electrolysis using a gel electrolyte. *J Power Sources* 2011; 196:2773–8.
- [10] Boggs BK, King RL, Botte GG. Urea electrolysis: direct hydrogen production from urine. *Chem Commun* 2009; 4859–61.
- [11] Daramola DA, Singh D, Botte GG. Dissociation rates of urea in the presence of NiOOH catalyst: a DFT analysis. *J Phys Chem A* 2010; 114:11513–21.
- [12] Sha L, Ye K, Wang G, et al. Hierarchical NiCo<sub>2</sub>O<sub>4</sub> nanowire array supported on Ni foam for efficient urea electrooxidation in alkaline medium. *J. Power Sources* 2019; 412:265–71.
- [13] Tong Y, Chen P, Zhang M, et al. Oxygen vacancies confined in nickel molybdenum oxide porous nanosheets for promoted electrocatalytic urea oxidation. *ACS Catal* 2018; 8:1–7.
- [14] Alajami M, Yassin MA, Ghouri ZK, et al. Influence of bimetallic nanoparticles composition and synthesis temperature on the electrocatalytic activity of NiMn-incorporated carbon nanofibers toward urea oxidation. *Int J Hydrogen Energy* 2018; 43:5561–75.
- [15] Shi W, Ding R, Li X, et al. Enhanced performance and electrocatalytic kinetics of Ni-Mo/graphene nanocatalysts towards alkaline urea oxidation reaction. *Electrochim Acta* 2017; 242:247–59.
- [16] Barakat NAM, El-Newehy MH, Yasin AS, et al. Ni&Mn nanoparticles-decorated carbon nanofibers as effective electrocatalyst for urea oxidation. *Appl Catal A: Gen* 2016; 510:180–8.
- [17] Xu W, Wu Z, Tao S. Urea-based fuel cells and electrocatalysts for urea oxidation. *Energy Technol* 2016; 4:1329–37.
- [18] Guo F, Ye K, Du M, et al. Electrochemical impedance analysis of urea electro-oxidation mechanism on nickel catalyst in alkaline medium. *Electrochim Acta* 2016; 210:474–82.
- [19] Lu S, Pan J, Huang A, et al. Alkaline polymer electrolyte fuel cells completely free from noble metal catalysts. *Proc Nat Acad Sci* 2008; 105:20611–4.
- [20] Bates MK, Jia Q, Ramaswamy N, et al. Composite Ni/NiO–Cr<sub>2</sub>O<sub>3</sub> catalyst for alkaline hydrogen evolution reaction. *J Phys Chem C* 2015; 119:5467–77.
- [21] Gu Y, Luo J, Liu Y, et al. Synthesis of bimetallic Ni–Cr nanooxides as catalysts for methanol oxidation in NaOH solution. *J Nanosci Nanotechnol* 2015; 15:3743–9.
- [22] Singh RK, Schechter A. Electroactivity of NiCr catalysts for urea oxidation in alkaline electrolyte. *ChemCatChem* 2017; 9:3374–9.
- [23] Vedharathnam V, Botte GG. Understanding the electrocatalytic oxidation mechanism of urea on nickel electrodes in alkaline medium. *Electrochim Acta* 2012; 81:292–300.
- [24] Zhu D, Guo C, Liu J, et al. Two-dimensional metal-organic frameworks with high oxidation states for efficient electrocatalytic urea oxidation. *Chem Commun* 2017; 53:10906–9.
- [25] Kim J, Choi WJK, Choi J, et al. Electrolysis of urea and urine for solar hydrogen. *Catal Today* 2013; 199:2–7.
- [26] Xu X, Gao J, Hong W. Ni-based chromite spinel for high-performance supercapacitors. *RSC Adv* 2016; 6:29646–53.
- [27] Bai YK, Zheng RT, Gu Q, et al. One-step synthesis of hollow Cr(OH)<sub>3</sub> micro/nano-hexagonal pellets and the catalytic properties of hollow Cr<sub>2</sub>O<sub>3</sub> structures. *J Mater Chem A* 2014; 2:12770–5.
- [28] Li W, Li Y, Wang H, et al. Co<sub>3</sub>S<sub>8</sub>-porous carbon spheres as bifunctional electrocatalysts with high activity and stability for oxygen reduction and evolution reactions. *Electrochim Acta* 2018; 265:32–40.
- [29] Taotao F, Hancheng Q, Meining Z. Co@C nanoparticle embedded hierarchically porous N-Doped hollow carbon for efficient oxygen reduction. *Chem Eur J* 2018; 24:1–9.
- [30] Bao X, Gong Y, Deng J, et al. Organic-acid-assisted synthesis of a 3D lasagna-like Fe-N-doped CNTs-G framework: an efficient and stable electrocatalyst for oxygen reduction reactions. *Nano Res* 2017; 10:1258–67.
- [31] Zhao J, Li X, Cui G, Sun X. Highly-active oxygen evolution electrocatalyzed by an Fe-doped NiCr<sub>2</sub>O<sub>4</sub> nanoparticle film. *Chem Commun* 2018; 54:5462–5.
- [32] Fu S, Zhu C, Su D, et al. Porous carbon-hosted atomically dispersed iron-nitrogen moiety as enhanced electrocatalysts for oxygen reduction reaction in a wide range of pH. *Small* 2018; 14:e1703118.
- [33] Zhao J, Ren X, Han Q, et al. Ultra-thin wrinkled NiOOH–NiCr<sub>2</sub>O<sub>4</sub> nanosheets on Ni foam: an advanced catalytic electrode for oxygen evolution reaction. *Chem Commun* 2018; 54:4987–90.
- [34] Tang T, Gan Q, Guo X, et al. A hybrid catalyst of Pt/CoNiO<sub>2</sub> on carbon nanotubes and its synergetic effect towards remarkable ethanol electro-oxidation in alkaline media. *Sustain Energy Fuels* 2018; 2:229–36.
- [35] Huajie X, Jing C, Changfu S, et al. MOF-derived hollow CoS decorated with CeO<sub>x</sub> nanoparticles for boosting oxygen evolution reaction electrocatalysis. *Angew Chem Int Ed* 2018; 57:1–6.
- [36] Shi Y, Zhou Y, Yang D-R, et al. Energy level engineering of MoS<sub>2</sub> by transition-metal doping for accelerating hydrogen evolution reaction. *J Am Chem Soc* 2017; 139:15479–85.
- [37] Liu S-Q, Wen H-R, Ying G, et al. Amorphous Ni(OH)<sub>2</sub> encounter with crystalline CuS in hollow spheres: a mesoporous nano-shelled heterostructure for hydrogen evolution electrocatalysis. *Nano Energy* 2018; 44:7–14.
- [38] Gan Q, Cheng X, Chen J, et al. Temperature effect on crystallinity and chemical states of nickel hydroxide as alternative superior catalyst for urea electrooxidation. *Electrochim Acta* 2019; 301:47–54.

- [39] Shih Y-J, Huang Y-H, Huang CP. Electrocatalytic ammonia oxidation over a nickel foam electrode: Role of Ni(OH)<sub>2</sub>(s)-NiOOH(s) nanocatalysts. *Electrochim Acta* 2018; 263:261–71.
- [40] Bian L, Du Q, Luo M, et al. Monodisperse nickel nanoparticles supported on multi-walls carbon nanotubes as an effective catalyst for the electro-oxidation of urea. *Int J Hydrogen Energy* 2017; 42:25244–50.
- [41] Zhao J, Ren X, Han Q, et al. Ultra-thin wrinkled NiOOH-NiCr<sub>2</sub>O<sub>4</sub> nanosheets on Ni foam: an advanced catalytic electrode for oxygen evolution reaction. *Chem Commun* 2018; 54:4987–90.
- [42] Wu M-S, Jao C-Y, Chuang F-Y, et al. Carbon-encapsulated nickel-iron nanoparticles supported on nickel foam as a catalyst electrode for urea electrolysis. *Electrochim Acta* 2017; 227:210–6.
- [43] Wang D, Liu S, Gan Q, et al. Two-dimensional nickel hydroxide nanosheets with high-content of nickel(III) species towards superior urea electro-oxidation. *J Electroanal Chem* 2018; 829:81–7.
- [44] Zhu X, Dou X, Dai J, et al. Metallic nickel hydroxide nanosheets give superior electrocatalytic oxidation of urea for fuel cells. *Angew Chem Int Ed Engl* 2016; 55:12465–9.
- [45] Jafarian M, Forouzandeh F, Danaee I, et al. Electrocatalytic oxidation of glucose on Ni and NiCu alloy modified glassy carbon electrode. *J Solid State Electrochem* 2009; 13:1171–9.
- [46] Bian L, Du T, Du Q, et al. Multiwalled carbon nanotubes twined α-nickel hydroxide microspheres as high-efficient urea electrooxidation catalysts. *J Appl Electrochem* 2017; 47:905–15.